



RESEARCH ARTICLE | MARCH 16 2022

Study on surface leakage current at sidewall in InP-based avalanche photodiodes with mesa structure

Junqin Zhang   ; Aofei Liu; Hailong Xing; Yintang Yang



AIP Advances 12, 035336 (2022)

<https://doi.org/10.1063/5.0080656>



AIP Advances

Why Publish With Us?



25 DAYS
average time
to 1st decision



740+ DOWNLOADS
average per article



INCLUSIVE
scope

[Learn More](#)



Study on surface leakage current at sidewall in InP-based avalanche photodiodes with mesa structure

Cite as: AIP Advances 12, 035336 (2022); doi: 10.1063/5.0080656

Submitted: 2 December 2021 • Accepted: 26 February 2022 •

Published Online: 16 March 2022



View Online



Export Citation



CrossMark

Junqin Zhang,^{a)}  Aofei Liu, Hailong Xing, and Yintang Yang

AFFILIATIONS

Key Laboratory of Ministry of Education for Wide Band Gap Semiconductor Materials and Devices, School of Microelectronics, Xidian University, Xi'an 710071, China

^{a)} Author to whom correspondence should be addressed: zhangjq@mail.xidian.edu.cn

ABSTRACT

A multi-mesa InGaAs/InP avalanche photodiode (APD) with the advantage of the completely restricted electric field is proposed. The surface defects, which are the reasons for the sidewall leakage current generation in the mesa-structure APD, are theoretically studied, and then a sidewall leakage current model is developed. The Silvaco Atlas device simulation tool is used to analyze the generation mechanism of the sidewall leakage current, and the effects of different mesa structures on the sidewall leakage current of the APD are compared. The simulation results show that the sidewall leakage current of the multi-mesa APD is about zero and is not affected by the terrace size, which can be contributed by a very weak electric field at the sidewall.

© 2022 Author(s). All article content, except where otherwise noted, is licensed under a Creative Commons Attribution (CC BY) license (<http://creativecommons.org/licenses/by/4.0/>). <https://doi.org/10.1063/5.0080656>

I. INTRODUCTION

At present, there are two main types of avalanche photodiode (APD) structures, including the planar structures and the mesa structures. In the planar structures, the epitaxial layer is deposited on a substrate highly doped by metal-organic chemical vapor deposition (MOCVD), and the top contact layer is formed by the Zn diffusion process. In the mesa structures, after epitaxial growth, only the etching process is needed to form a mesa structure, and the fabrication process is simple.¹ In particular, in a large-scale array APD, the planar structure has poor uniformity and repeatability due to the diffusion process instability; in contrast, the mesa structure has the advantages of good device uniformity, repeatability, stability, and reliability, which can be contributed by the simple etching process; thus, the mesa structure is more suitable for large-scale APD arrays.

However, a relatively high dark current is a severe problem that seriously affects device performance, thus limiting the large-scale application of APDs with the mesa structure. The dark current of the mesa-structure APD is mainly composed of two types of current components: the bulk dark current and the surface leakage

current. The bulk dark current is mainly related to the material quality, while the surface leakage current mainly relies on the surface process. The etching process is necessary to form a mesa structure, which results in a large number of defects on the APD surface caused by dangling bonds, crystal defects, and impurities. These surface defects cause surface leakage current, which significantly increases the dark current in InGaAs/InP APD, especially at the sidewall of the InGaAs layer. Therefore, passivation of the sidewalls is particularly important in mesa-structure APDs. Accordingly, many passivation materials, such as Si₃N₄, SiO₂, BCB, SU-8, and polyimide, have been explored. In particular, these materials have been deposited on the surface of the mesa to reduce the surface leakage current.²⁻⁵ However, these methods can reduce only some of the surface defects but cannot eliminate the influence of surface defects on the dark current.⁶ According to Ref. 7, the dark current of the mesa-structure APD is higher than that of the planar-structure APD, mainly because of the insufficient passivation. Recently, many low-dark-current InAlAs-based triple-mesa APDs have been reported, which suppress part of the sidewall leakage current, thereby reducing the total dark current.⁸⁻¹¹ However, few studies have described the generation mechanism of surface leakage current.¹²

In this paper, a multi-mesa InGaAs/InP avalanche photodiode, which has the advantage of the completely restricted electric field, is proposed. The influencing factors of the surface leakage current are studied, and the generation mechanism of sidewall leakage current is explained in detail. In addition, the dark current in the APDs with different structures is compared in the same active region and at the same device thickness and doping concentration, and the contributions of the sidewall leakage current to the total dark current are also obtained.

II. DEVICE STRUCTURE AND SURFACE LEAKAGE CURRENT MODEL

The schematic cross-sectional views of three mesa-structure APDs, which have the same epitaxial layers in this work, are depicted

in Fig. 1. On the InP substrate, the following layers are deposited sequentially: the *n*-type InP contact layer, intrinsic In_{0.53}Ga_{0.47}As absorption layer, *n*-type InGaAsP grading layer, *n*-type InP charge layer, intrinsic InP multiplication layer, *p*-type InP charge layer, lightly doped edge-field buffer layer, and heavily doped *p*-type contact layer. The detailed parameters for each layer are shown in Table I. The presented multi-mesa APD contains four mesas, which increase in size from the top to the bottom. The *p*-type contact layer is the first mesa. The edge-field buffer layer and *p*-type charge layer constitute the second mesa, and the careful design of the two layers can avoid the local breakdown at the mesa edge. The third mesa contains the multiplication layer, *n*-type charge layer, grading layer, and absorption layer. The *n*-type contact layer, which is mainly used for electrode isolation between devices, represents the fourth mesa.

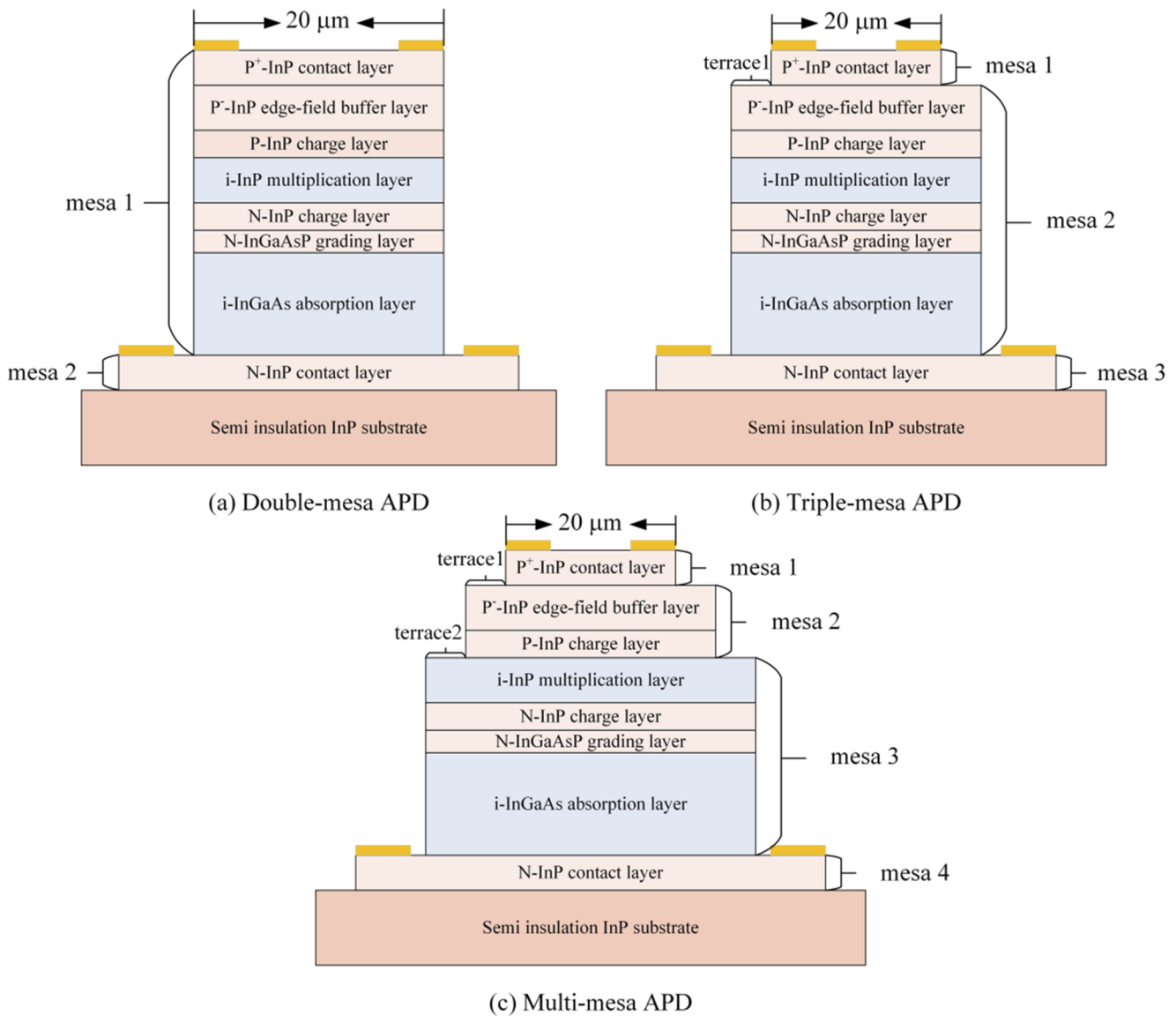


FIG. 1. The schematic cross-sectional views of three mesa-structure APDs.

TABLE I. Structural parameters of three mesa-structure APDs.

	Thickness (μm)	Doping concentration (cm^{-3})
p^+ -InP contact layer	0.5	1×10^{18}
p^- -InP edge-field buffer layer	0.5	5×10^{15}
p -InP charge layer	0.1	3×10^{17}
i -InP multiplication layer	0.16	1×10^{15}
n -InP charge layer	0.1	3×10^{17}
n -InGaAsP grading layer	0.05	1×10^{16}
i -In _{0.53} Ga _{0.47} As absorption layer	2	1×10^{15}
n -InP contact layer	0.5	1×10^{17}
Semi-insulation InP substrate	3	1×10^{14}

Meanwhile, terraces are formed at the edge-field buffer layer and multiplication layer, and they are denoted as the terraces 1 and 2, respectively.

In the mesa-structure APDs, the dark current includes not only the bulk dark current that is generated inside the device but also the surface leakage current that is generated at the mesa edge. Therefore, the dark current density of a mesa-structure APD is given by¹³

$$J_d \times A = J_{\text{bulk}} \times A + J_{\text{surf}} \times p, \quad (1)$$

where J_d denotes the total dark current density, J_{bulk} denotes the bulk dark current density, and J_{surf} denotes the surface leakage current density at the device sidewall; A represents the surface area of the active region, and p is the perimeter of the sidewall. The surface leakage current is essentially a type of surface recombination current caused by surface defects. Surface defects can form the defect energy levels on the semiconductor surface, further generating surface charges or recombination centers, increasing the surface recombination.

This paper mainly considers the surface leakage current generated at the sidewalls of the InP multiplication layer and InGaAs absorption layer. In the mesa-structure InGaAs/InP APDs, the InGaAs absorption layer occupies the largest sidewall surface. Moreover, InGaAs is a material with a narrow bandgap, and surface recombination is more likely to occur in this layer. Accordingly, the InGaAs absorption region is one of the main sources of the sidewall leakage current in mesa-structure APDs.¹⁴ Although the multiplication layer is InP, which is a wide-bandgap material, surface recombination still exists in actual devices because the strongest electric field of a device is the one in the multiplication layer. Hence, the sidewall leakage current in the InP multiplication layer cannot be ignored.¹⁵

In the fabrication process of mesa-structure APDs, etching is required to form mesas. After dry etching, the device surface is damaged, and defect energy levels are introduced, which increases the surface recombination at the sidewalls and thereby increases the surface leakage current. As reported in Ref. 16, when wet etching was performed after dry etching, surface damage could be eliminated, and a surface as that of the un-etched would be obtained. However, an un-etched surface still has surface states caused by unsaturated dangling bonds and point defects caused by impurities, vacancies,

and antisite atoms.¹⁷ The surface states can be reduced or even eliminated by saturating the dangling bonds conducting the passivation and annealing processes.¹⁸ However, the point defects that originate from the InGaAs and InP themselves cannot be eliminated by passivation,¹⁹ and they are the main reason for the surface leakage current.

In the InGaAs/InP heterojunction avalanche photodiodes, the epitaxial growth is usually along with the crystal orientation [100]. This is because of the sphalerite structure, such as that of InGaAs or InP, where the crystal plane (110) is a cleavage plane and the crystal plane (100) is perpendicular to the crystal plane (110). By using the crystal plane (100) as an epitaxial growth plane, the crystal plane (110) can be conveniently used as a cleavage plane. As for the InP (110) surface, in Ref. 17, it was indicated that the properties of III-V compound semiconductors were significantly affected by defects, and the formation mechanism of point defects was studied by using a scanning tunneling microscope (STM). It was concluded that the thermal creation of P^- vacancies was the main formation mechanism of surface defects, and the highest concentration of vacancies is $5 \times 10^{12} \text{ cm}^{-2}$. The work of Dow and Allen showed that the defect energy levels formed by the P^- vacancy were close to the conduction band edge, and they were not deep levels but shallow donor levels.²⁰ In Ref. 21, it was demonstrated that surface charges caused by P^- vacancies existed on the InP surface, and the charge on the n -type doped InP surface was negative. This was because each P^- vacancy represented a positive charge center that formed the bound energy level of electrons. These energy levels were located in the forbidden band and captured electrons. The vacancies had a net charge of at most one electron.²² When there were thermal excitation or electric field, the electrons captured by the P^- vacancy defect levels would be released into the conduction band within a certain thickness of the InP surface and would become free electrons, making the n -type InP surface become the electron accumulation layer.¹²

In Ref. 23, the interface state distribution of the In_{0.53}Ga_{0.47}As-oxide interface was measured by admittance spectroscopy, and two main peaks were observed, one was close to the valence band and another one was in the middle of the bandgap. The interface state distribution was not affected by the passivation, surface cleanliness, and annealing processes, so the surface defects originated from InGaAs itself. Reference 23 also explains that inherent surface defects may be high-concentration vacancies at the surface.

The defect energy levels caused by the vacancies denote deep donor energy levels, and they act as recombination centers and affect the surface recombination velocity. Thus, both the surface charge of the InP sidewall and the surface recombination center of the InGaAs sidewall increase the surface recombination rate, resulting in a large sidewall surface leakage current.

The three mesa-structure InGaAs/InP APDs were modeled by the Silvaco Atlas in which the numerical calculation is based on a series of basic equations and physical models. For simulating the current–voltage (I–V) characteristics of the APD, the physical models, including the basic drift-diffusion model, generation-recombination model, tunneling model, and impact ionization model, were applied. The generation–recombination processes included four generation-recombination mechanisms: Auger, radiation, Shockley–Read–Hall (SRH), and surface generation-recombination. On the other hand, the tunneling process included indirect trap-assisted tunneling (TAT) and direct band-to-band tunneling (BBT). For more specific information on the above models, see Refs. 24–27 and the Silvaco Atlas user manual.²⁸

In Silvaco, the surface recombination rate is defined as²⁴

$$R_{surf} = \frac{pn - n_i^2}{\tau_{sp}[n + n_i \exp(\frac{E_i - E_T}{kT})] + \tau_{sn}[p + n_i \exp(\frac{E_T - E_i}{kT})]}, \quad (2)$$

where n_i denotes the intrinsic carrier concentration; n and p are the electron concentration and hole concentration in a device surface, respectively; E_i and E_T are the intrinsic Fermi level and recombination center level, respectively; k denotes the Boltzmann constant; and T is the lattice temperature in degrees Kelvin. τ_{sp} and τ_{sn} are the hole lifetimes and electronic lifetimes due to the surface recombination, and they are, respectively, related to the recombination velocity for the hole and electron. The surface charge density and surface recombination velocity are user-definable in the Silvaco Atlas.

III. SIMULATION RESULTS AND DISCUSSION

A. Surface leakage current at sidewall of double-mesa APD

The traditional double-mesa APD represents the simplest mesa-structure APD in which, as the reverse bias voltage increases, the electric field at the sidewall stays almost the same as that in the center. Although the fabrication process is simple because there is no diffusion process, the sidewall surface leakage current is large due to the strong electric field at the sidewall. Therefore, the sidewall leakage current of a double-mesa APD was first studied for understanding the generation mechanism of the sidewall leakage current.

First, the sidewall leakage current of the InGaAs absorption layer was ignored, and only the sidewall leakage current in the InP multiplication layer was considered. The reverse I–V characteristic that varies with the surface charge density of the multiplication layer is shown in Fig. 2(a). As presented in Fig. 2(a), when the surface charge of the multiplication layer was less than $7 \times 10^{11} \text{ cm}^{-2}$, the dark current changed slightly with the surface charge. However, when the surface charge was larger than $7 \times 10^{11} \text{ cm}^{-2}$, the dark current increased significantly, and the increase was more obvious at high reverse bias voltage. When the surface charge density of the multiplication layer was $5 \times 10^{11} \text{ cm}^{-2}$, the dark current changed slightly with the bias voltage in the range of 20–43 V. However, when the surface charge density of the multiplication layer was $1 \times 10^{12} \text{ cm}^{-2}$ and the bias voltage was about 32 V, the dark current increased significantly. Thus, both the sidewall electric field and the surface charge of the multiplication layer are the main factors affecting the sidewall leakage current. Therefore, the sidewall leakage current in the multiplication layer can be decreased by reducing the surface defects or the sidewall electric field.

The dark current that varies with the surface charge density of the multiplication layer at a different reverse bias voltage is shown

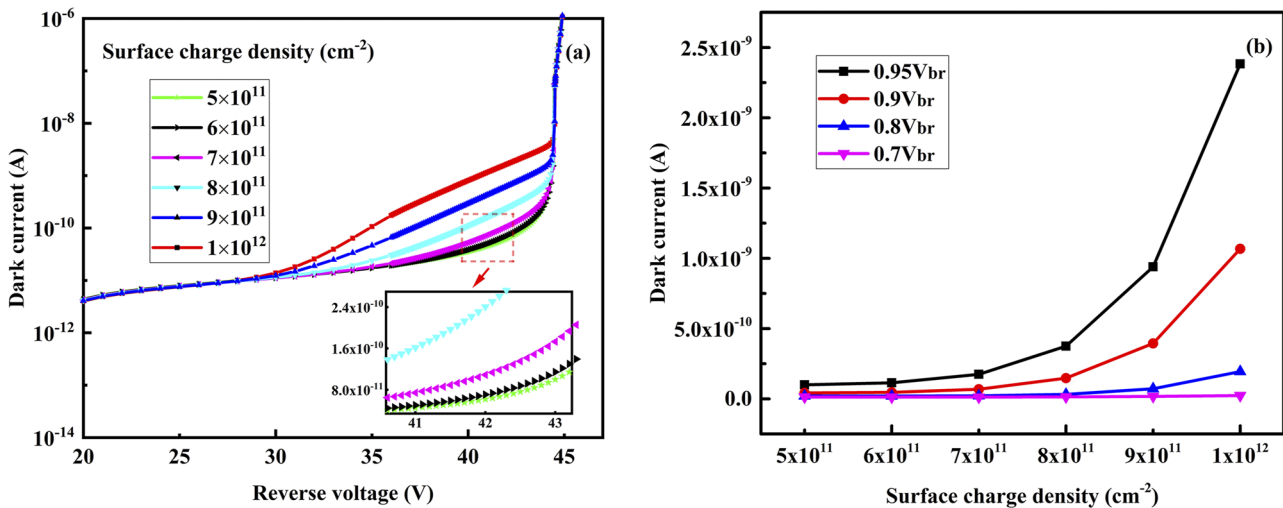


FIG. 2. (a) The reverse I–V characteristics of the double-mesa APD at a different surface charge density of the multiplication layer; (b) the dark current varies with the surface charge density at a different reverse bias voltage.

in Fig. 2(b). In Fig. 2(b), it can be observed that the increase in the dark current with the surface charge density at the bias voltage of $0.95V_{br}$ (here, V_{br} denotes the breakdown voltage) was larger than that at the bias voltage of $0.7V_{br}$. Thus, the impact of surface charge on the dark current at high voltage was much larger than that at low bias voltage, further indicating that part of the surface charge of the multiplication layer participated in impact ionization. At the bias voltage of $0.95V_{br}$, when the surface charge density of the multiplication layer was larger than $7 \times 10^{11} \text{ cm}^{-2}$, the dark current increased significantly. However, at the bias voltage of $0.9V_{br}$, only when the surface charge density was larger than $8 \times 10^{11} \text{ cm}^{-2}$, the dark current increased obviously. Thus, at different reverse bias voltages, only when the surface charge density was larger than a certain value, the dark current changed significantly. This was related to the sidewall electric field of the multiplication layer, namely, the stronger the electric field was, the higher the impact ionization rate was. Therefore, even a slightly lower surface charge density would also have a great effect on the dark current.

Similarly, the sidewall leakage current in the multiplication layer was ignored, and only the sidewall leakage current of the absorption layer was considered. The reverse I–V characteristics at a different surface recombination velocity of the InGaAs absorption layer are presented in Fig. 3(a). In Fig. 3(a), it can be seen that when the APD was not punch-through (here, it means the bias voltage less than 16 V), the dark current did not change with the surface recombination velocity. This was because the absorption layer was not depleted, and there was no sidewall electric field at the absorption layer. However, when the APD was penetrated, the dark current increased with the surface recombination velocity. Thus, it can be obtained that when the sidewall of the absorption layer is depleted, the sidewall leakage current can be decreased by reducing the surface defects of the absorption layer. Accordingly, if the zero sidewall electric field in the absorption layer can be achieved by optimizing the APD structure, the sidewall leakage current in the absorption layer

can be avoided. The dark current change with the surface recombination velocity of the absorption layer at the bias voltage of $0.9V_{br}$ is displayed in Fig. 3(b). The results showed that when the surface recombination velocity was smaller than $1 \times 10^3 \text{ cm/s}$, the dark current increased slowly, but the dark current increases rapidly at the surface recombination velocity of larger than $1 \times 10^3 \text{ cm/s}$.

In summary, the sidewall leakage current in the multiplication layer is related to the surface charge and sidewall electric field. A part of the surface charge participates in impact ionization. When the surface charge of the multiplication layer is more than $7 \times 10^{11} \text{ cm}^{-2}$ and the bias voltage exceeds 32 V, a sidewall surface leakage current will be generated, and it will have a significant contribution to the total dark current. The sidewall leakage current in the absorption layer depends on the surface recombination center. When the sidewall of the absorption layer is depleted, the sidewall leakage current increases with the surface recombination velocity, showing a significant increase at the surface recombination velocity of more than $1 \times 10^3 \text{ cm/s}$.

B. Dependence of surface leakage current at sidewall of mesa-structure APD

In an actual device, defects are often randomly distributed onto the device surface, so the surface charge of the multiplication layer and the surface recombination center of the absorption layer will simultaneously affect the sidewall leakage current. In further analysis, the surface charge density of the multiplication layer and surface recombination velocity of the absorption layer were, respectively, set to $1 \times 10^{12} \text{ cm}^{-2}$ and $1 \times 10^4 \text{ cm/s}$.

The dark current in different structure APDs is presented in Fig. 4. The dark current when the surface factors at the sidewall were and were not considered is shown in Figs. 4(a) and 4(b), respectively. In Fig. 4(b), the dark currents of the three APDs are almost the same, which indicates that the mesa structure type does not affect the bulk

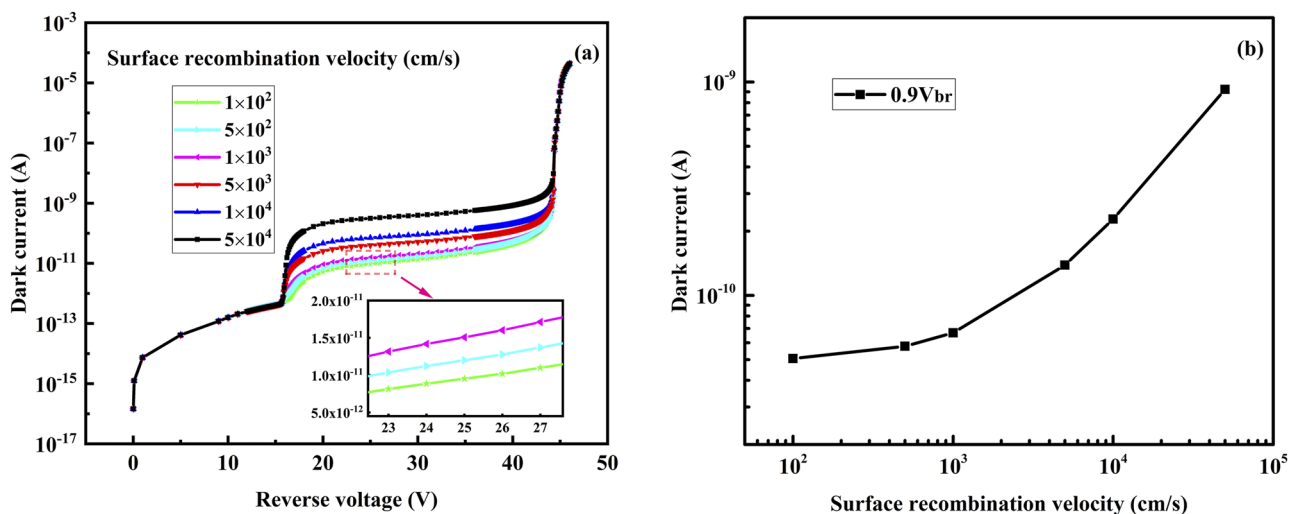


FIG. 3. (a) The reverse I–V characteristics of the double-mesa APD at a different surface recombination velocity of the absorption layer; (b) the dark current varies with the surface recombination velocity at the bias voltage of $0.9V_{br}$.

dark current. This result was caused by the same active regions in the three APDs. On the contrary, in Fig. 4(a), the dark currents of the three APDs are different; namely, the dark current of the double-mesa APD is the highest and that of the multi-mesa APD is the lowest. These results demonstrate that APD structure has a great impact on the sidewall leakage current, thereby affecting the total dark current. This can be explained by the sidewall electric field.

The sidewall electric fields of the three APDs are extracted at several different reverse bias voltages. Figure 5 shows the electric field distribution of the APDs at 10 and 46 V bias voltage. Due to the strong sidewall electric field of the multiplication layer in the double-mesa APD, as depicted in Fig. 5(b), the surface charge participates in impact ionization, which increases the dark current significantly when the bias voltage is larger than 32 V. When the bias voltage is about 10 V, the sidewall of the absorption layer in the double-mesa APD is depleted, as depicted in Fig. 5(a), so the surface recombination in the absorption layer also increases the dark current. Due to a weaker sidewall electric field of the multiplication layer in the triple-mesa APD, as depicted in Fig. 5(b), the contribution of the sidewall leakage current in the multiplication layer to the dark current is small even at high reverse bias voltage. However, there also exists some sidewall electric field in the absorption layer at a bias voltage of about 10 V, as depicted in Fig. 5(a), so the sidewall leakage current of the absorption layer is the main part of the sidewall leakage current in the triple-mesa APD. It should be noted that the terrace width of the triple-mesa APD is $5 \mu\text{m}$. As the sidewall electric field of the multiplication layer in the multi-mesa APD is the lowest not enough to cause the impact ionization and the sidewall of the absorption layer has not been depleted at a high reverse bias voltage, as depicted in Fig. 5(b), the sidewall leakage current in the multi-mesa APD is almost zero.

To sum up, compared to both the double-mesa APD and the triple-mesa APD, the multi-mesa APD has the advantage of almost completely restricting the electric field, which makes the sidewall electric field very weak. Therefore, even if there exist surface defects,

the sidewall leakage current can be neglected, thus achieving a low dark current. By comparing the dark current of the multi-mesa APD and the planar APD, we found that they were almost the same. This is because the application of the selective doping technology in the planar APD also restricts the electric field to the device center.

C. Effect of terrace size on surface leakage current at sidewall in mesa-structure APD

The triple- and multi-mesa APDs can restrict the electric field to the device center due to the existence of the terrace. Therefore, the effect of the terrace width on the dark current was studied. The surface charge density of the multiplication layer and the surface recombination velocity of the absorption layer were, respectively, set to $7 \times 10^{11} \text{ cm}^{-2}$ and $1 \times 10^4 \text{ cm/s}$.

At the bias voltage of $0.9V_{br}$, the total dark current and the bulk dark current in the triple-mesa APD vary with the terrace width, as shown in Fig. 6(a). As presented in Fig. 6(a), the bulk dark current increased slightly with the terrace width. However, the total dark current decreased significantly with the increase in the terrace width, which indicated that the terrace width of the triple-mesa APD mainly affected the sidewall leakage current. This is related to the sidewall electric field of the device. The extracted sidewall electric field distribution at a different terrace width at the bias voltage of $0.9V_{br}$ is presented in Fig. 6(b). When the terrace width is less than $4 \mu\text{m}$, the sidewall leakage current decreases with the reduction in the sidewall electric field of the multiplication layer. When the terrace width is larger than $4 \mu\text{m}$, the sidewall electric field in the multiplication layer is already low not enough to make the surface charge cause impact ionization, thereby not generating a significant sidewall leakage current in the multiplication layer. The sidewall leakage current is mainly originating from the absorption layer.

For the triple-mesa APD, the smaller the terrace size is, the higher the dark current will be. In addition, both the absorption layer

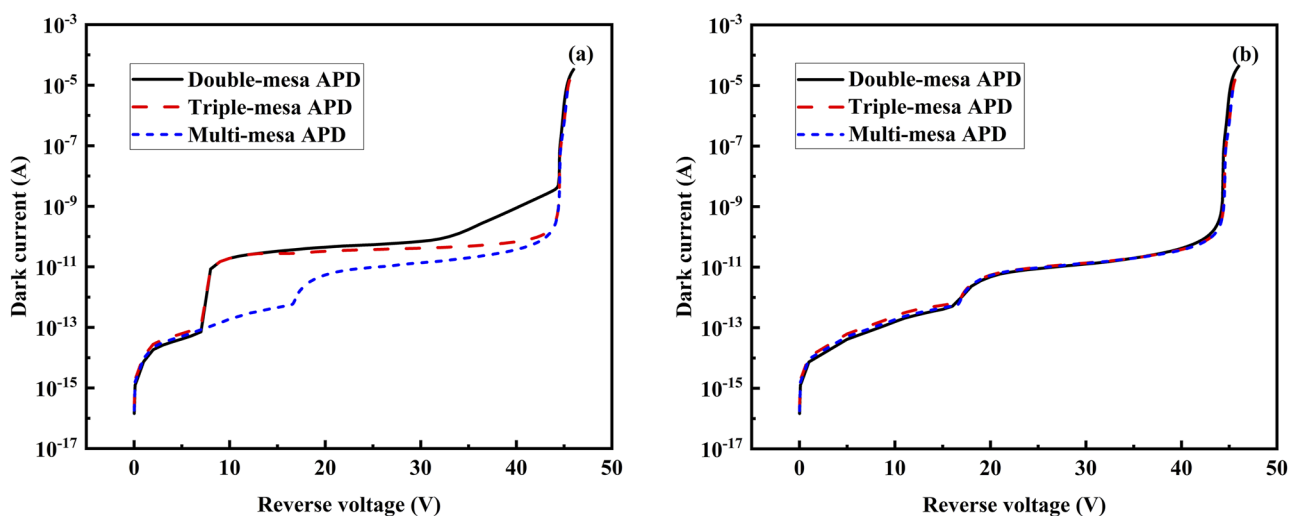


FIG. 4. Comparison of dark current of different APDs: (a) considering the surface factors and (b) without considering the surface factors.

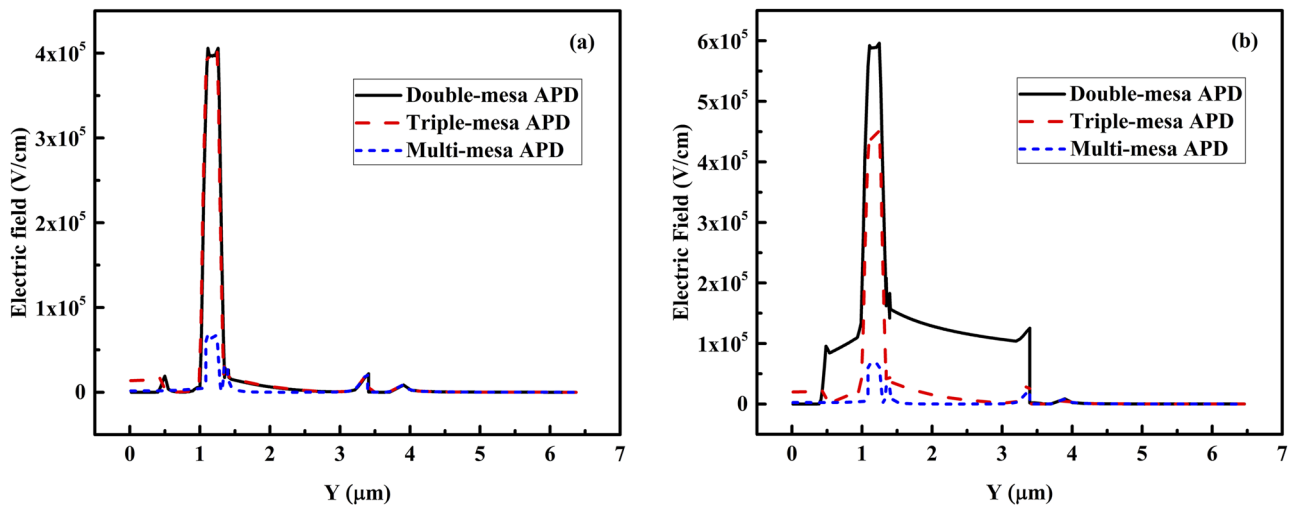


FIG. 5. The sidewall electric field of the three APDs at a (a) 10 V bias voltage and (b) 46 V bias voltage.

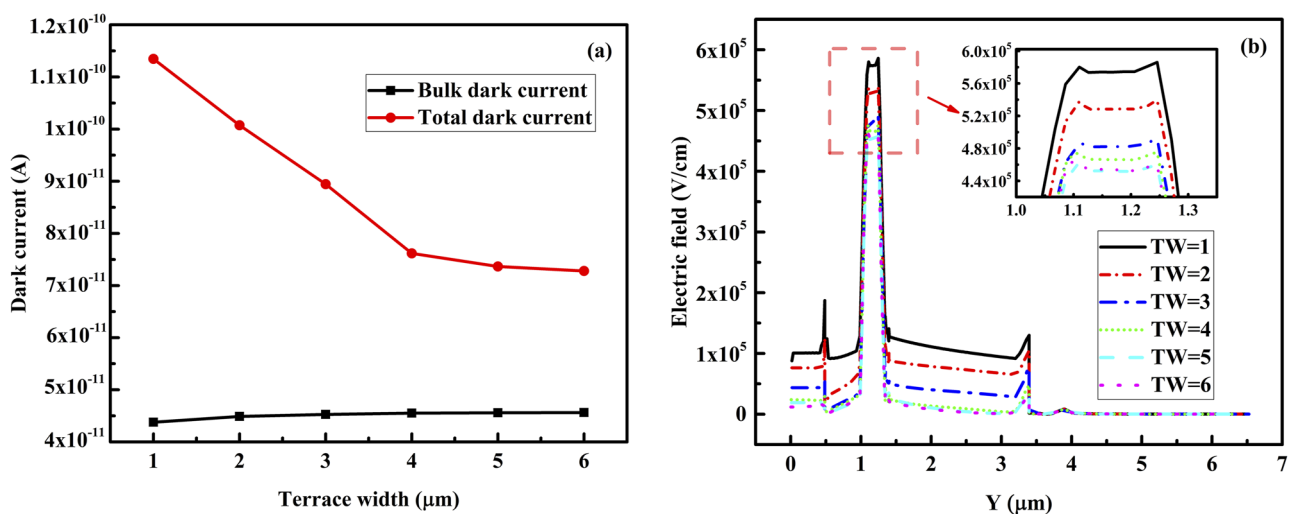


FIG. 6. (a) The bulk dark current and the total dark current at different terrace widths of the triple-mesa APD; (b) the sidewall electric field distribution at the bias voltage of $0.9V_{br}$.

and the multiplication layer contribute to the sidewall leakage current. When the terrace size is more than $4 \mu\text{m}$, the sidewall leakage current in the multiplication layer can be negligible, but there is still some sidewall leakage current in the absorption layer. However, the dark current of the multi-mesa APD is not affected by the terrace size because the sidewall leakage current in the multi-mesa APD is zero.

IV. CONCLUSION

The surface charges in the InP multiplication layer, and the surface recombination centers in the InGaAs absorption layer, resulting

from the intrinsic semiconductor defects, are the main reasons for the generation of the sidewall leakage current in the mesa structure APDs. Parts of the surface charge participate in impact ionization, and when the surface charge and reverse bias voltage are large enough, the sidewall leakage current in the multiplication layer will be generated. If the sidewall of the absorption layer is depleted, the sidewall leakage current in the absorption layer will increase with the surface recombination velocity, showing a significant increase at the surface recombination velocity of more than 1×10^3 cm/s. Based on this, the dark currents of APDs with different structures are compared, and the contribution of the sidewall leakage current to the total dark current is discussed. It is found that the structure

type has a great impact on the sidewall leakage current. This impact is the highest in the double-mesa APD and the lowest in the multi-mesa APD. Finally, the influence of terrace size on the dark current is studied. The research results show that the terrace size significantly affects the sidewall leakage current of the triple-mesa APD, but the dark current of the multi-mesa APD stays unchanged with the terrace size.

ACKNOWLEDGMENTS

This work was financially supported by the National Natural Science Foundation of China (Grant Nos. 61834004 and 62134005).

AUTHOR DECLARATIONS

Conflict of Interest

The authors declare that they have no conflicts of interest to disclose.

DATA AVAILABILITY

The data that support the findings of this study are available from the corresponding author upon reasonable request.

REFERENCES

- ¹J.-J. Liu, W.-J. Ho, C.-C. Chiang, C.-J. Teng, C.-C. Yu, and Y.-C. Li, *Sensors* **18**, 2800 (2018).
- ²T. Tansel, K. Kutluer, Ö. Salihoglu, A. Aydinli, B. Aslan, B. Arikan, M. C. Kilinc, Y. Ergun, U. Serincan, and R. Turan, *IEEE Photonics Technol. Lett.* **24**, 790 (2012).
- ³H. S. Kim, J. H. Choi, H. M. Bang, Y. Jee, S. W. Yun, J. Burm, M. D. Kim, and A. G. Choo, *Electron. Lett.* **37**, 455 (2001).
- ⁴H. S. Kim, E. Plis, A. Khoshakhlagh, S. Myers, N. Gautam, Y. D. Sharma, L. R. Dawson, S. Krishna, S. J. Lee, and S. K. Noh, *Appl. Phys. Lett.* **96**, 033502 (2010).
- ⁵J.-J. Liu, W.-J. Ho, J.-Y. Chen, J.-N. Lin, C.-J. Teng, C.-C. Yu, Y.-C. Li, and M.-J. Chang, *Sensors* **19**, 3399 (2019).
- ⁶Y. Ma, Y. Zhang, Y. Gu, X. Chen, Y. Shi, W. Ji, S. Xi, B. Du, X. Li, H. Tang, Y. Li, and J. Fang, *Opt. Express* **24**, 7823 (2016).
- ⁷K. Circir, M. H. Dolas, and S. Kocaman, *Infrared Phys. Technol.* **97**, 360 (2018).
- ⁸Y. Yuan, Y. Li, J. Abell, J. Zheng, K. Sun, C. Pinzone, and J. C. Campbell, *Opt. Express* **27**, 22923 (2019).
- ⁹Y. H. Chen, J. M. Wun, S. L. Wu, R. L. Chao, J. J. S. Huang, Y. H. Jan, H. S. Chen, C. J. Ni, H. S. Chang, E. Chou, and J. W. Shi, *IEEE J. Sel. Top. Quantum Electron.* **24**, 3800208 (2018).
- ¹⁰B. Li, Q.-Q. Lv, R. Cui, W.-H. Yin, X.-H. Yang, and Q. Han, *IEEE Photonics Technol. Lett.* **27**, 34 (2015).
- ¹¹M. Nada, Y. Muramoto, H. Yokoyama, T. Ishibashi, and H. Matsuzaki, *J. Lightwave Technol.* **32**, 1543 (2014).
- ¹²Q. Y. Zeng, W. J. Wang, J. Wen, L. Huang, X. H. Liu, N. Li, and W. Lu, *J. Appl. Phys.* **115**, 164512 (2014).
- ¹³X. Ji, B. Liu, H. Tang, X. Li, M. Shi, Y. Zhou, Y. Xu, H. Gong, and F. Yan, *Jpn. J. Appl. Phys.* **54**, 04DG09 (2015).
- ¹⁴M. Nada, Y. Muramoto, H. Yokoyama, N. Shigekawa, T. Ishibashi, and S. Kodama, *Jpn. J. Appl. Phys.* **51**, 02BG03 (2012).
- ¹⁵G. Liu, X. Wang, J. Zhao, W. Chen, Y. Tian, and J. Yang, *Opt. Commun.* **435**, 374 (2019).
- ¹⁶Y. Q. Lv, F. Y. Yue, X. K. Hong, J. F. Chen, B. Han, X. L. Wu, and H. M. Gong, *Chin. J. Semicond.* **28**, 122 (2007), <https://kns.cnki.net/kcms/detail/detail.aspx?FileName=BDTX200701025&DbName=CJFQ2007>.
- ¹⁷M. Heinrich, Ph. Ebert, M. Simon, K. Urban, and M. G. Lagally, *J. Vac. Sci. Technol. A* **13**, 1714 (1995).
- ¹⁸H. J. Tang, X. L. Wu, K. F. Zhang, Y. F. Li, J. H. Ning, Y. Wang, X. Li, and H. M. Gong, *Appl. Phys. A* **91**, 651 (2008).
- ¹⁹H.-P. Komsa and A. Pasquarello, *Physica B* **407**, 2833 (2012).
- ²⁰J. D. Dow and R. E. Allen, *J. Vac. Sci. Technol.* **20**, 659 (1982).
- ²¹Ph. Ebert, K. Urban, and M. G. Lagally, *Phys. Rev. Lett.* **72**, 840 (1994).
- ²²M. D. Pashley, K. W. Haberern, and R. M. Feenstra, *J. Vac. Sci. Technol. B* **10**, 1874 (1992).
- ²³G. Brammert, H. C. Lin, K. Martens, A.-R. Alian, C. Merckling, J. Penaud, D. Kohen, W.-E. Wang, S. Sioncke, A. Delabie, M. Meuris, M. R. Caymax, and M. Heyns, *ECS Trans.* **19**, 375 (2009).
- ²⁴V. Gopal, W. Qiu, and W. Hu, *J. Appl. Phys.* **116**, 184503 (2014).
- ²⁵J. W. Parks, A. W. Smith, K. F. Brennan, and L. E. Tarof, *IEEE Trans. Electron Devices* **43**, 2113 (1996).
- ²⁶X. D. Wang, W. D. Hu, X. S. Chen, W. Lu, H. J. Tang, T. Li, and H. M. Gong, *Opt. Quantum Electron.* **40**, 1261 (2008).
- ²⁷A. Liu, J. Zhang, H. Xing, and Y. Yang, *Appl. Opt.* **58**, 5339 (2019).
- ²⁸Device Simulation Software, *ATLAS User's Manual* (Silvaco Inc., Santa Clara, CA, 2010).